# Diagnostic and Imaging Approaches to Chest Wall Lesions

*Joseph Mansour, MD*
*Demetrios Raptis, MD*
*Sanjeev Bhalla, MD*
*Allen P. Heeger, DO*
*Gerald F. Abbott, MD*
*Nadeem Parkar, MD*
*Mark M. Hammer, MD*
*Julia Kiernan, MD*
*Constantine Raptis, MD*

**Abbreviations:** FDG = fluorodeoxyglucose, MO =myositis ossificans, MPNST = malignant peripheral nerve sheath tumor, SAPHO = *s*ynovitis, *a*cne, *p*ustulosis, *h*yperostosis, and *o*steitis

**RadioGraphics 2022; 42:359–378**

**https://doi.org/10.1148/rg.210095**

**Content Codes:** CH CT MK MR

From the Mallinckrodt Institute of Radiology, Washington University School of Medicine, St Louis, Mo (J.M., D.R., S.B., C.R.); Department of Radiology, Massachusetts General Hospital, Boston, Mass (A.P.H., G.F.A.); Department of Radiology, Cleveland Clinic, Cleveland, Ohio (N.P.); Department of Radiology, Brigham and Women's Hospital, Boston, Mass (M.M.H.); and Department of Radiology, St Louis University Hospital, St Louis, Mo (J.K.). Recipient of a Certificate of Merit award for an education exhibit at the 2020 RSNA Annual Meeting. Received March 29, 2021; revision requested May 10 and received June 3; accepted June 10. For this journal-based SA-CME activity, the authors S.B. and M.M.H. have provided disclosures (see end of article); all other authors, the editor, and the reviewers have disclosed no relevant relationships. **Address correspondence to** J.M., Department of Radiology and Imaging Sciences, Indiana University, 550 N University Blvd, Room 0634, Indianapolis, IN 46202 (e-mail: *joseph.mansour001@gmail.com*).



## SA-CME LEARNING OBJECTIVES

*After completing this journal-based SA-CME activity, participants will be able to:*

- Recognize various chest wall lesions and their characteristic imaging findings.
- Discuss the diagnosis and management of different chest wall lesions.
- Identify the imaging findings and clinical clues that can aid in making the appropriate diagnosis.

*See rsna.org/learning-center-rg.*

Chest wall lesions are relatively uncommon and may be challenging once they are encountered on images. Radiologists may detect these lesions incidentally at examinations performed for other indications, or they may be asked specifically to evaluate a suspicious lesion. While many chest wall lesions have characteristic imaging findings that can result in an accurate diagnosis with use of imaging alone, other entities are difficult to distinguish at imaging because there is significant overlap among them. The interpreting radiologist should be familiar with the imaging features of both "do not touch" benign entities (which can be confidently diagnosed with imaging only, with no need for biopsy or resection unless the patient is symptomatic) and lesions that cannot be confidently characterized and thus require further workup. CT and MRI are the main imaging modalities used to assess the chest wall, with each having different benefits and drawbacks. Chest wall lesions can be classified according to their predominant composition: fat, calcification and ossification, soft tissue, or fluid. The identification or predominance of signal intensities or attenuation for these findings, along with the patient age, clinical history, and lesion location, can help establish the appropriate differential diagnosis. In addition, imaging findings in other organs, such as the lungs or upper abdomen, can at times provide clues to the underlying diagnosis. The authors review different chest wall lesions classified on the basis of their composition and highlight the imaging findings that can assist the radiologist in narrowing the differential diagnosis and guiding management.



## Introduction

Benign and malignant chest wall lesions account for 5% of all thoracic tumors (1). Making the diagnosis on the basis of imaging findings alone is challenging, as there is significant overlap of imaging appearances among the different lesions. While imaging may not lead to a specific diagnosis, it can help narrow the differential diagnosis to further direct diagnostic workup, management, and treatment. Imaging allows the classification of chest wall lesions based on their attenuation or signal intensity, which may be that of fat, calcification and ossification, fluid, or soft tissue (Table 1). A systematic approach to imaging chest wall lesions, combined with assessment of the clinical features, can help direct patient care (Table 2).

## TEACHING POINTS

- A well-differentiated liposarcoma showing interval development of a T2-hyperintense area that enhances after contrast material administration suggests a dedifferentiated liposarcoma.
- Corticomedullary continuity with the parent bone is diagnostic of osteochondroma.
- Elastofibroma dorsi typically has linear areas of fat within the tumor, which are sometimes termed the *lasagna sign* because of the layering appearance.
- With aggressive fibromatosis, the mass is generally heterogeneous on CT images but can have the same attenuation as muscle; in these cases, the clue that a desmoid tumor is present is focal or asymmetric enlargement of a single muscle.
- MRI findings are often diagnostic of hematoma when a fluid-fluid level is seen within a fluid collection.

## Imaging Modalities

Chest wall lesions are frequently detected incidentally on images. Chest radiography is rarely useful but may allow visualization of chest wall lesions that involve the osseous thorax or contain calcifications. These findings are usually more evident on dedicated rib views obtained by using a technique involving a lower kilovoltage, as opposed to standard chest radiography (2). Depending on their size and location, larger noncalcified lesions or extraosseous lesions can be seen on radiographs occasionally. US is useful for detecting palpable or superficial lesions and offers the benefit of the lack of ionizing radiation. It mainly serves to help guide biopsy and avoid vessels.

Cross-sectional imaging is the best way to further evaluate chest wall lesions. CT and MRI enable assessment of the location, composition, and enhancement characteristics of suspicious and incidental lesions. CT is superior to MRI in depicting calcification and enables better delineation of the osseous thorax. MRI provides greater contrast resolution of soft-tissue lesions. Owing to the advent of surface coils, high-quality MRI of chest wall lesions can now be performed. MRI is the modality of choice for evaluating pleural, mediastinal, or organ invasion. Moreover, MRI enables better tissue characterization and better assessment of nerve and vessel involvement. Often, especially with more complex lesions, both CT and MRI are performed.

Fluorodeoxyglucose (FDG) PET/CT can prove to be valuable in planning tissue sampling to target the region of the lesion that has the most FDG uptake and avoid necrotic areas of the tumor. In addition, FDG PET/CT is useful for pretreatment planning to identify distant extrathoracic metastases, as patients with more advanced stages of disease require medical therapy and are not ideal candidates for surgical resection. However, there is substantial overlap in FDG uptake between benign and malignant chest wall lesions, so the degree of FDG uptake should not be used to make a diagnosis (3).

## Fat-containing Lesions

### Benign Lesions

Lipomas are the most common fat-containing lesions of the chest wall, with a higher prevalence in patients older than 50 years (4). These neoplasms are composed of adipose tissue and are frequently encapsulated by a thin layer of fibrous tissue. Lipomas have the attenuation and signal intensity of normal subcutaneous fat on CT and MR images, respectively. Fat-suppressed MRI sequences can be used to distinguish lipomas from other lesions or structures that may demonstrate similar signal intensity on a given non–fat-suppressed MR image (Fig 1). Lipomas are generally homogeneous without nodular enhancement, but they may contain thin enhancing septa that are less than 2 mm in thickness, or calcification in up to one-third of cases (5). When lipomas occur in the chest wall, they are more likely to occur in the deeper soft tissues than in the subcutaneous fat (2). Intramuscular lipomas are a potential pitfall, as these nonencapsulated lesions can occasionally mimic liposarcomas, demonstrating an infiltrative and striated appearance owing to intermingled muscle fibers (6).

Spindle cell lipomas are less common fat-containing lesions that usually occur in the subcutaneous fat of the neck or shoulder in men older than 45 years (7). Histologically, these tumors consist of mature adipocytes, uniform spindle cells, and bundles of collagen. In these fat-containing heterogeneous tumors that enhance after contrast material administration, the spindle cells account for the nonfatty areas (7). At imaging, a spindle cell lipoma usually manifests as a well-defined fat-containing lesion with areas of enhancement (Fig 2). These lesions are often resected, as their appearance is similar to that of low-grade liposarcomas at imaging.

Other less common benign fat-containing lesions include hibernomas and lipoblastomas. Hibernomas are benign encapsulated neoplasms that contain brown fat. They are difficult to distinguish from well-differentiated liposarcomas, as they contain areas of soft tissue and may have subtle enhancement. These lesions tend to occur in regions where brown fat is commonly found, including the interscapular region, axillae, and chest wall (8). MRI findings include well-circumscribed masses with mildly heterogeneous fat signal intensity and thin internal strands. These

**Table 1: Chest Wall Lesions**

| Lesion Type | Benign Lesions* | Malignant Lesions |
|---|---|---|
| Fat containing | Lipoma, spindle cell lipoma, hibernoma, lipoblastoma (in children) | Liposarcoma |
| Calcified and ossified | Fibrous dysplasia, MO, tumoral calcinosis, dermatomyositis and polymyositis Scleroderma, osteochondra, SAPHO syndrome | Chondrosarcoma, osteosarcoma |
| Fluid | Hematoma, lymphatic malformation, abscess, empyema necessitans, aneurysmal bone cyst, seroma or lymphocele | Cystic or necrotic metastasis |
| Soft tissue | Peripheral nerve sheath tumor, elastofibroma dorsi, vascular malformation, aggressive fibromatosis | Sarcomas, metastasis, myeloma or plasmacytoma, malignant nerve sheath tumor |

*MO = myositis ossificans, SAPHO = *s*ynovitis, *a*cne, *p*ustulosis, *h*yperostosis, and *o*steitis.

**Table 2: Management of Chest Wall Lesions**

| Lesion Type | "Do Not Touch" Lesions* | Resection or Surgery | Biopsy | Medical or Other Therapy |
|---|---|---|---|---|
| Fat containing | Lipoma | Liposarcoma | Indeterminate fatty lesion | … |
| Calcified and ossified | Osteochondroma, fibrous dysplasia, MO | Chondrosarcoma, osteosarcoma, malignant degeneration of osteochondroma | … | Dermatomyositis, scleroderma, SAPHO syndrome |
| Fluid | Hematoma | Aneurysmal bone cyst, abscess, lymphatic malformation | … | Infection, hematoma (reverse anticoagulation or embolization) |
| Soft tissue | Nerve sheath tumor, elastofibroma dorsi, hemangioma | MPNST,† aggressive fibromatosis, sarcoma (no metastasis), Ewing sarcoma (after chemoradiation) | Sarcoma, lymphoma, indeterminate mass | Stage IV malignancy, lymphoma |

*"Do not touch" lesions can be confidently diagnosed with imaging alone and thus do not require biopsy or resection unless the patient is symptomatic.
†MPNST = malignant peripheral nerve sheath tumor.

masses are hypointense to subcutaneous fat and may be completely suppressed on fat-saturated MR images (8). Hibernomas tend to drop out on opposed-phase–signal MR images. Biopsy can be used to confirm the diagnosis (8).

Lipoblastoma should be the leading differential consideration for a child younger than 3 years who has a fat-containing lesion of the chest wall (9). Lipoblastomas are difficult to distinguish from hibernomas with imaging alone, as lipoblastomas, which are predominantly fatty encapsulated tumors, also may have enhancing septa (Fig 3). While both hibernomas and lipoblastomas can mimic liposarcomas, it is important to be mindful that liposarcomas are exceedingly rare in individuals younger than 10 years (10).

Fat necrosis can be seen in the subcutaneous tissue of the chest wall, and it may lead to confusion, as most patients with fat necrosis do not recall a traumatic incident (11). On MR images, fat necrosis appears as a globular lesion containing a fatty core and surrounded by a hypointense rim. Calcification and fat stranding are sometimes seen. These lesions are often confused with malignant neoplasms such as liposarcoma owing to their imaging appearance and FDG uptake (12). Decreasing size at follow-up imaging can be a helpful clue to suggest this diagnosis.

## Malignant Lesions

After undifferentiated pleomorphic sarcoma, liposarcoma is the most common malignant soft-tissue

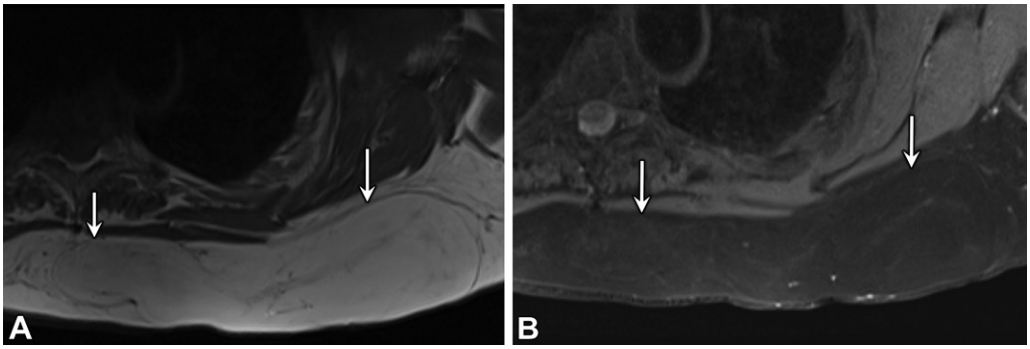


**Figure 1.** Lipoma in a 59-year-old woman who presented with a left chest mass that had been growing during the past year. Contrast-enhanced MRI of the chest was performed. Transaxial non–fat-saturated T1-weighted MR image **(A)** shows a hyperintense mass (arrows) that is nulled on the transaxial fat-saturated T1-weighted MR image **(B)**. The lesion showed no enhancement on contrast-enhanced MR images (not shown). Owing to its growth, the mass was resected, and pathologic analysis confirmed lipoma.

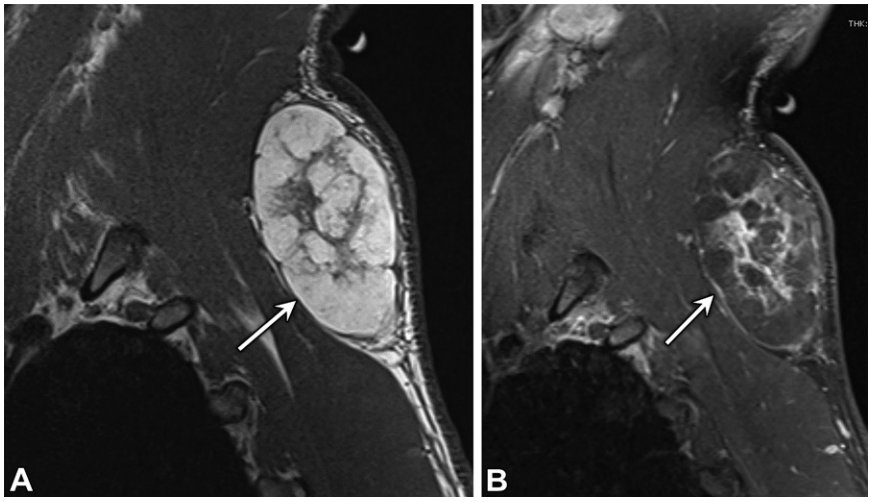


**Figure 2.** Spindle cell lipoma in a 42-year-old man who presented with a lump in the upper left chest wall. **(A)** Sagittal non–fat-saturated T1-weighted MR image shows a fat-containing mass (arrow) with multiple thick hypointense septa, which were also hyperintense at T2-weighted MRI (not shown). **(B)** Sagittal contrast-enhanced T1-weighted fat-saturated MR image shows enhancement of the thick septa in the mass (arrow). The mass was excised owing to concern for liposarcoma, and spindle cell lipoma was found.

chest wall tumor (13). In the World Health Organization classification system, the most common types of liposarcomas are described: well differentiated, dedifferentiated, myxoid, pleomorphic, and mixed (14). The different subtypes of liposarcoma can be thought of as a spectrum from least to most differentiated. The more differentiated the tumor, the more fat it contains and the less aggressive it is (Table 3). Conversely, the more undifferentiated tumors have less or sometimes no fat and are more aggressive.

The well-differentiated subtype is the most common, accounting for approximately half of liposarcomas. On images, these tumors contain a large amount of fat, which can account for 50%–75% of the tumor volume (15). Well-differentiated liposarcomas have an appearance similar to that of lipomas in up to 9% of cases (16). MRI findings that help differentiate well-differentiated liposarcoma from lipoma include septa that are greater than 2 mm in thickness, nodular soft-tissue areas, larger size (>10 cm), and fat encompassing less than 75% of the tumor (15). A well-differentiated liposarcoma showing interval development of a T2-hyperintense area that enhances after contrast material administration suggests a dedifferentiated liposarcoma (4). This occurs with approximately 10% of well-differentiated liposarcomas (14).

Myxoid liposarcomas represent approximately 20%–50% of liposarcomas and comprise less than 25% fat (17). Myxoid areas usually have a high water content, manifesting as fluid-like high signal intensity on T2-weighted MR images (Fig 4) and as hypoattenuation on CT images (4). Calcification and ossification can be seen with all subtypes of liposarcoma, but most commonly with the well-differentiated

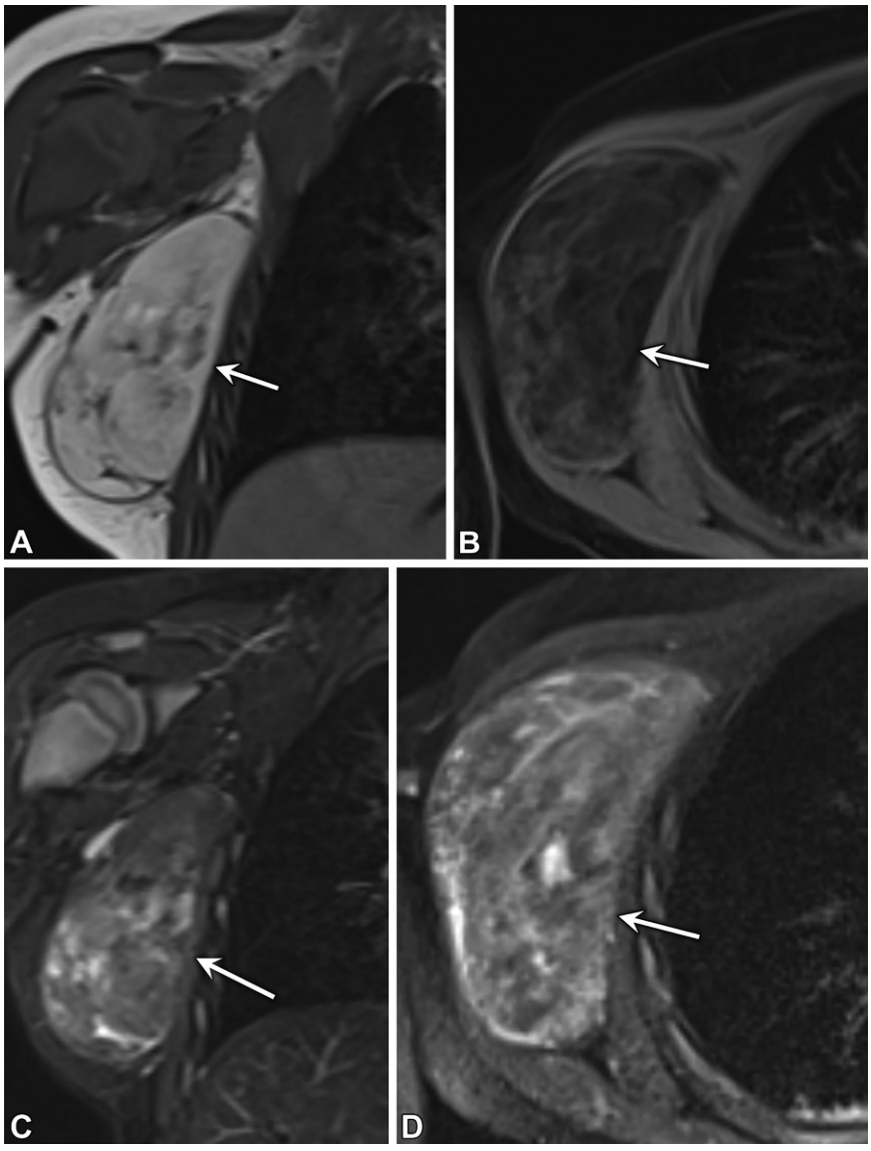


**Figure 3.** Lipoblastoma in a 2-year-old boy who had a palpable mass in the right axilla and underwent contrast-enhanced MRI. **(A, B)** Coronal T1-weighted non–fat-saturated image **(A)** shows areas of hyperintensity (arrow), which are suppressed on the transaxial T1-weighted fat-saturated image **(B)**. **(C, D)** Coronal T2-weighted short τ inversion-recovery image **(C)** shows multiple hyperintense septa in the mass (arrow), with corresponding enhancement on the transaxial contrast-enhanced T1-weighted fat-saturated image **(D)**. The mass was resected, and pathologic analysis revealed lipoblastoma.

subtype (13). However, calcification can also be seen with lipomas (15). If percutaneous biopsy is needed, the nonadipose components should be targeted. The most aggressive form of liposarcoma, the pleomorphic subtype, is the least common and appears as a heterogeneous soft-tissue mass on CT and MR images. Given that 62%–75% of pleomorphic liposarcomas contain no fat (17), differentiating them from other soft-tissue sarcomas is difficult.

## Calcified and Ossified Lesions

Calcified and ossified lesions can occur in the soft tissues or arise from bone. Approximately 95% of primary osseous tumors of the chest wall arise from the ribs, and the majority of the remainder of these tumors arise from the sternum (18). Among the ossified and calcified chest wall neoplasms, fibrous dysplasia is the most common benign tumor and chondrosarcoma is the most common malignant tumor (19).

### Benign Lesions

Fibrous dysplasia occurs secondary to a developmental anomaly in which normal marrow and bone are replaced by fibrous stroma. Usually an incidental finding, fibrous dysplasia can result in a pathologic fracture or rarely, malignant

degeneration. The ribs are a common location, and imaging demonstrates an intramedullary, expansile, long-segment, well-defined lesion. These lesions may demonstrate endosteal scalloping and cortical thinning; however, the cortex remains intact. Fibrous dysplasia occurs most commonly in the lateral or posterior aspect of the ribs (1), with a characteristic "bubbly cystic" appearance on radiographs and CT images. These lesions show varying degrees of hazy ground-glass matrix. However, they may appear nearly entirely lucent or sclerotic, depending on the degree of fibrous component. At MRI, fibrous dysplasia tends to be hypointense to muscle on T1-weighted images and hypo- or hyperintense on T2-weighted images (Fig 5). Enhancement is variable, depending on the histologic composition (20).

Osteochondromas are common osseous lesions that occur secondary to aberrant growth of normal bone tissue. These neoplasms are often singular and sporadic, but multiple lesions can occur with hereditary conditions such as Trevor disease and hereditary multiple exostoses. Osteochondromas frequently occur in the ribs, most commonly at the costochondral junction, but they can also arise from the scapula or spine (2).

Corticomedullary continuity with the parent bone is diagnostic of osteochondroma (Fig 6). MRI might show a characteristic T2-hyperintense cartilaginous cap. Patients with multiple osteochondromas have a 2.7%–5.0% lifetime risk of malignant degeneration, most commonly degeneration into chondrosarcoma (21,22). These patients may present with pain associated with the osteochondroma. At imaging, malignant degeneration should be suspected if the cartilaginous cap increases in thickness (to >2 cm) or if irregular calcifications or mineralization, or osseous erosion develops (2,23,24).

*Tumoral calcinosis* refers to soft-tissue calcification that occurs in the setting of end-stage renal disease or chronic inflammatory conditions. These calcifications are typically found adjacent to joints and can be symmetric. Other clues at chest imaging can help suggest the diagnosis. These clues include atrophic kidneys in the partially imaged upper abdomen, subchondral bone resorption at the sternoclavicular joints, diffuse vascular calcifications, and increased bone density. Fluid-calcium levels also have been reported in the calcifications, with higher attenuation in the dependent portion of the calcification (25,26). Myositis ossificans (MO) is a specific type of heterotopic ossification that occurs in muscle after trauma. The term *myositis* is a misnomer, as this entity is not inflammatory. In the first 4–8 weeks, MO has the appearance of a soft-tissue mass with floccular density. Once MO matures, usually by 2 months, the characteristic imaging finding of a soft-tissue lesion with peripheral calcification is seen (26). This peripheral calcification can be useful in distinguishing MO from parosteal osteosarcomas, which tend to have central calcification. Early MO can enhance and be mistaken for sarcoma; in this scenario, follow-up imaging can be performed for a more definitive diagnosis (27). It should be noted that it is preferable not to perform biopsy of these lesions, as they have been reported to be mistaken for malignancy at histopathologic analysis (28,29).

Connective tissue disease such as scleroderma and dermatomyositis and polymyositis also can lead to soft-tissue calcification that is more punctate and dense than tumoral calcinosis. In scleroderma, these areas of dystrophic calcification are more commonly seen in the hands but can also occur in the chest wall (30). Other clues to scleroderma at chest imaging include a dilated esophagus and interstitial lung disease with a nonspecific interstitial pneumonia pattern (31). Dermatomyositis and polymyositis classically cause calcification of the fascia; patients with dermatomyositis also develop cutaneous calcification

**Table 3: Spectrum of Liposarcomas**

| |
|---|
| Liposarcomas that are less aggressive and more differentiated and contain more fat and less soft tissue |
| Well differentiated: |
| Most common (~50% of cases) |
| Occur in older adults (aged 50–70 y) |
| 50%–75% fat |
| Thick septa (>2 mm) |
| Nodular soft tissue (<1 cm) |
| Myxoid: |
| 20%–50% of liposarcomas |
| Occur in younger adults (in 4th–5th decade of life) |
| <25% fat |
| High water content (hyperintense on T2-weighted MR images) |
| Liposarcomas that are more aggressive and less differentiated and contain less fat and more soft tissue: |
| Pleomorphic: |
| Least common |
| Necrosis and hemorrhage |
| Can have no fat (62%–75% of cases) |
| Dedifferentiated: |
| Dedifferentiation from a well-differentiated liposarcoma (10% of cases) |
| Metastases to liver and lungs (15%–20% of cases) |

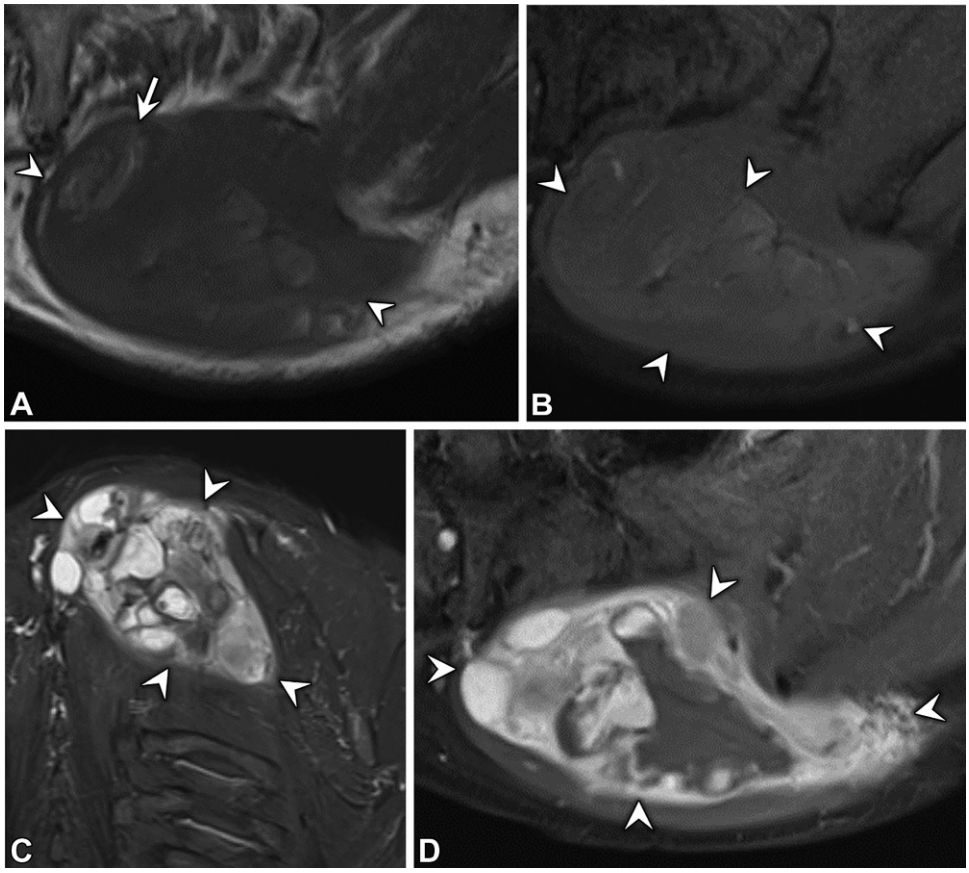


**Figure 4.** Myxoid liposarcoma in a 72-year-old man with a palpable mass involving the left upper back. **(A, B)** Transaxial non–fat-saturated T1-weighted MR image **(A)** shows a T1-hypointense mass (arrowheads) with areas of T1 hyperintensity (arrow in **A**), which are null on the transaxial fat-saturated T1-weighted MR image **(B). (C)** Coronal short τ inversion-recovery MR image shows areas of very hyperintense T2 signal, representing the myxoid areas of the lesion (arrowheads). **(D)** Transaxial contrast-enhanced fat-saturated T1-weighted MR image shows avid enhancement of the T2-hyperintense areas of the mass (arrowheads). The mass was resected, and histologic analysis confirmed myxoid liposarcoma.

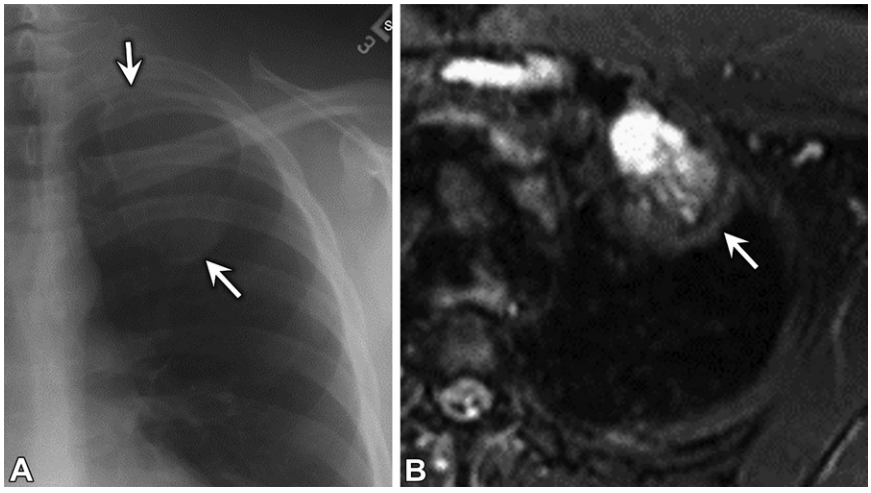


**Figure 5.** Fibrous dysplasia in a 37-year-old man. **(A)** Posteroanterior chest radiograph shows an incidentally discovered expansile mass (arrows) involving the left second rib, with ground-glass attenuation. **(B)** Transaxial T2-weighted fat-saturated MR image shows a hyperintense mass (arrow) in the left second rib that was hypointense at T1-weighted MRI (not shown). The mass was resected after biopsy revealed a spindle neoplasm. Findings at histologic analysis after resection confirmed fibrous dysplasia.

(Fig 7) (32). The calcification occurs as a healing response to recurrent episodes of necrosis (26). These patients often develop connective tissue disease–associated interstitial lung disease more commonly with a nonspecific interstitial pneumonia pattern (33,34).

SAPHO syndrome is a benign condition characterized by *s*ynovitis, *a*cne, *p*ustulosis, *h*yperostosis, and *o*steitis. The main imaging finding is hyperostosis of the sternoclavicular joints, which may be striking and raise suspicion for malignancy such as osteosarcoma or metastasis. On CT images, there is cortical thickening centered at the sternoclavicular joint, with intact cortical margins and narrowing of the medullary cavity. Involvement of the thoracic spine is highly suggestive of this syndrome (Fig 8). With active disease, marrow edema may be seen on T2-weighted MR images, while there is an absence of edema with chronic disease. The "bull's head" sign is a highly specific finding that is seen at delayed bone scintigraphy and characterized by radiotracer uptake in the sternoclavicular joints and the manubrium (35,36). Nonsteroidal anti-inflammatory agents, steroids, disease-modifying rheumatic drugs, and biologic agents are used to treat SAPHO syndrome (37).

### Malignant Lesions

Chondrosarcoma is the most common primary malignant neoplasm of the osseous chest wall and accounts for approximately one-third of tumors (4). Osteosarcoma of the chest wall is less common. Imaging features can help differentiate these two tumors. Chondrosarcoma tends to occur anteriorly, arising from the costochondral junction (Fig 9), which is by far the most common location, followed by the sternum and occasionally the scapula. Osteosarcomas tend to arise from the ribs, scapula, or clavicle (4,38). The pattern of mineralization is key in distinguishing these entities. A chondroid matrix, including arches and rings, stippled shapes, and flocculence, seen on radiographs and CT images is suggestive of chondrosarcoma. A more osseous-appearing matrix that manifests as dense, cloudy, and ivory like is suggestive of osteosarcoma (Fig 10). In addition, chondrosarcoma tends to have more peripheral calcification, whereas osteosarcoma has more central ossification (39). On T2-weighted MR images, chondrosarcomas are usually hyperintense owing to the presence of a cartilaginous matrix with high water content (Fig 11) (17,40). MRI is particularly useful for biopsy planning and to show local tumor extent for surgical planning. CT is useful to assess for metastatic disease, typically to the lungs.

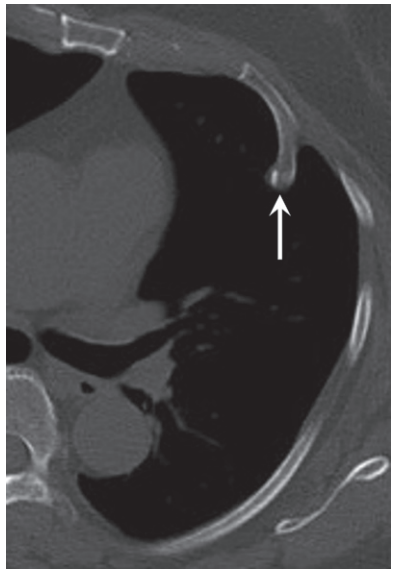

**Figure 6.** Osteochondroma found at lung cancer screening in a 66-year-old woman who smokes. Axial noncontrast CT image shows an osteochondroma (arrow) from the anterior left fourth rib with corticomedullary continuity.

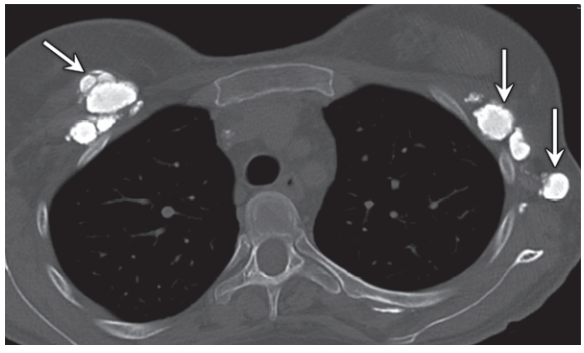

**Figure 7.** Dermatomyositis in a 25-year-old woman. Transaxial noncontrast chest CT image obtained to assess shortness of breath and concern for connective tissue disease–associated interstitial lung disease shows multiple soft-tissue calcifications (arrows).

## Soft-Tissue Lesions

### Definitely Benign Lesions

Elastofibroma dorsi lesions are classically located between the serratus anterior and latissimus dorsi, deep to the inferior aspect of the scapula. This lesion results from the accumulation of fibrotic tissue with elastic fibers. Elastofibromas are much more common in women and can occur bilaterally in up to two-thirds of cases (41). While these lesions are bilateral, the lesion on one side is typically larger than the lesion on the other side.

The appearance of elastofibroma dorsi on CT and MR images is pathognomonic, especially

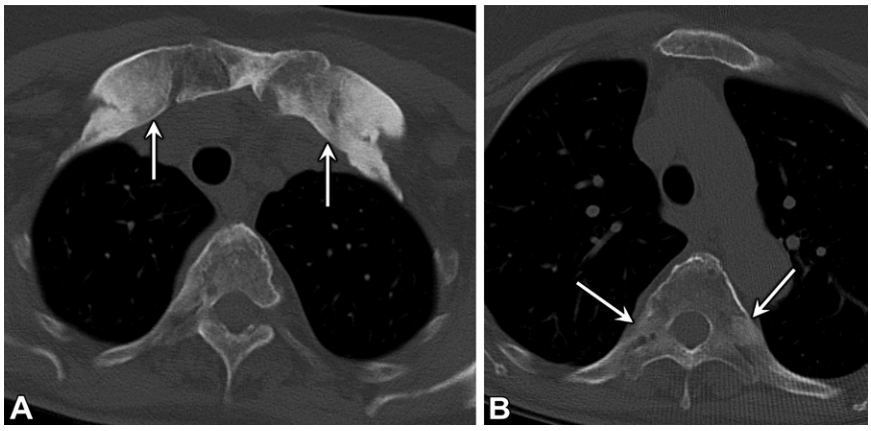


**Figure 8.** SAPHO syndrome in a 49-year-old man. Transaxial noncontrast CT images show hyperostosis and ankylosis at the sternoclavicular joint (arrows in **A**) and hyperostosis of the thoracic spine (arrows in **B**).

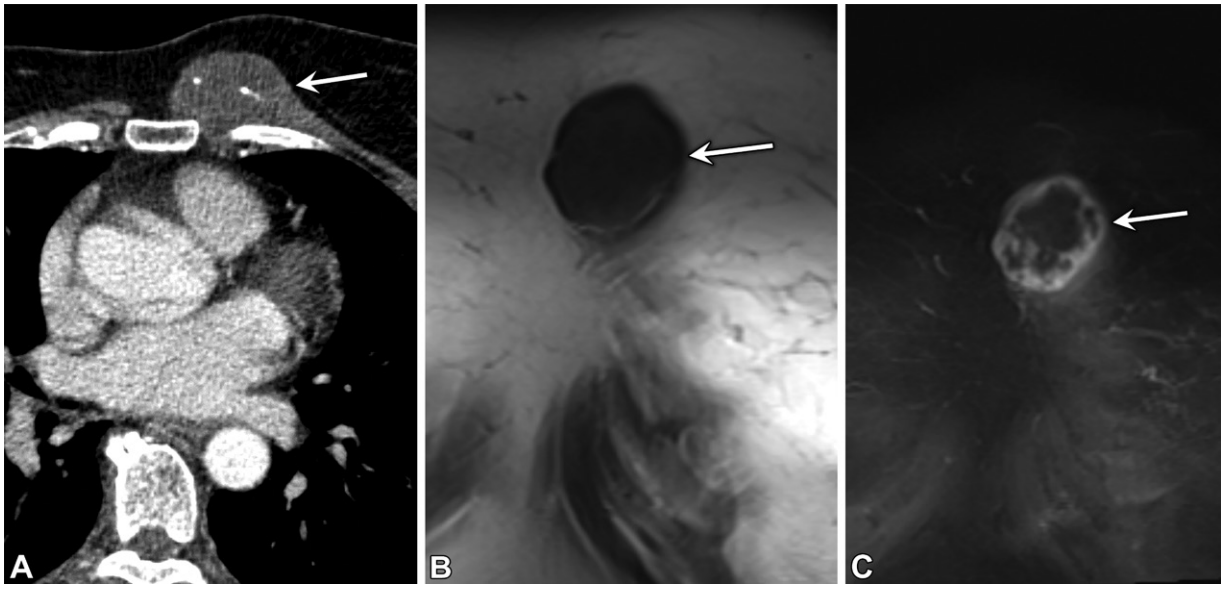


**Figure 9.** Chondrosarcoma in a 71-year-old woman. **(A)** Contrast-enhanced chest CT image obtained to assess a painful chest lump shows a mass (arrow) arising from the left anterior costochondral junction. The mass has central, punctate, and archlike calcifications (chondroid matrix). **(B)** Coronal noncontrast non–fat-saturated T1-weighted MR image shows a hypointense mass (arrow). **(C)** Coronal contrast-enhanced fat-saturated MR image shows peripheral nodular enhancement (arrow). Histopathologic analysis confirmed the diagnosis of chondrosarcoma.

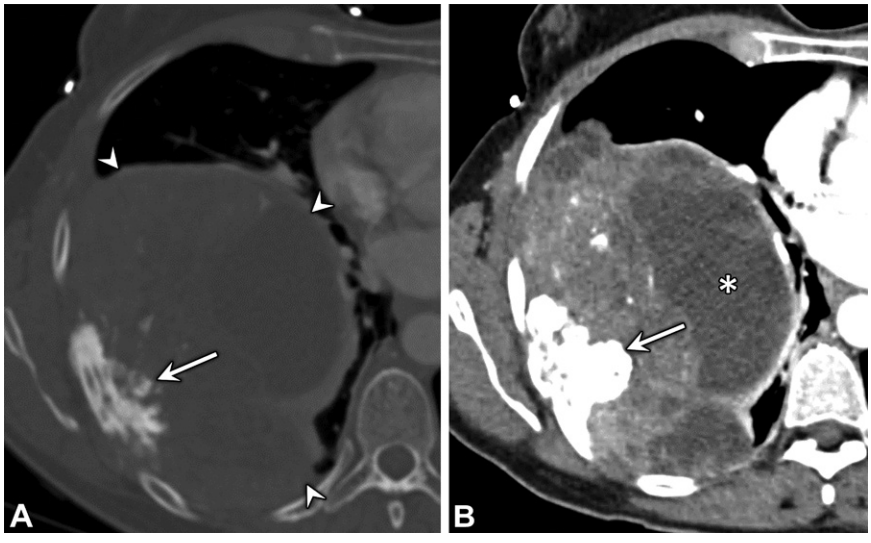


**Figure 10.** Osteosarcoma in a 42-year-old woman who had progressively worsening dyspnea and pain with breathing for the past 3 months. Chest radiography (not shown) revealed a large right hemithorax mass. **(A)** Transaxial contrast-enhanced CT image (bone window) shows a large mass (arrowheads) arising from the right fourth rib, with central ossification (arrow). **(B)** Transaxial CT image (soft-tissue window) shows a central ossified component (arrow) and enhancing soft tissue with cystic areas of necrosis (*). This mass was resected, and histologic analysis revealed high-grade osteosarcoma.

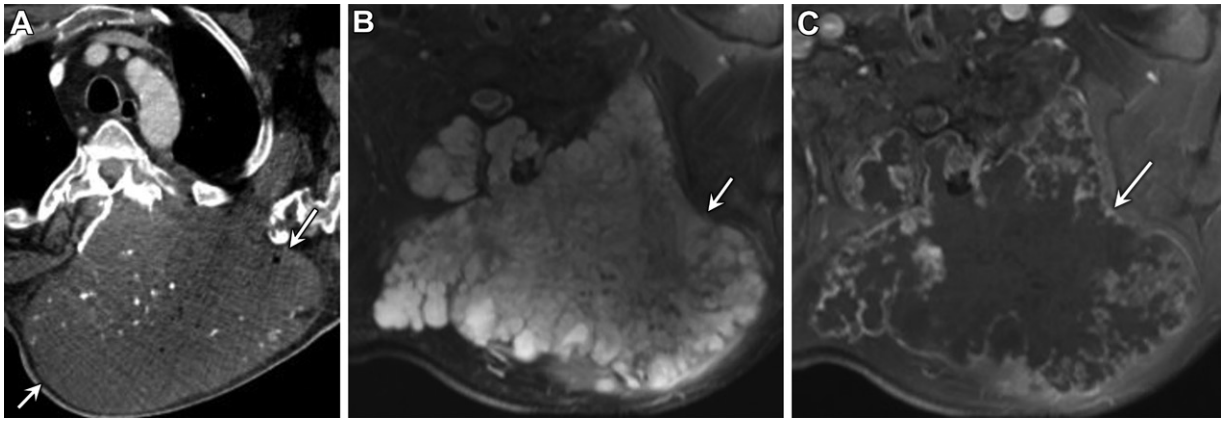


**Figure 11.** Chondrosarcoma arising from osteochondroma in a 57-year-old man with a history of hereditary osteochondromas who presented with a left upper back mass that had been slowly growing for the past 10 years. **(A)** Transaxial contrast-enhanced chest CT image shows a large mass (arrows) with a stippled chondroid matrix arising from an osteochondroma. The small locules of gas are secondary to biopsies performed the previous day. **(B)** Transaxial T2-weighted fat-saturated MR image shows a hyperintense mass (arrow). **(C)** Transaxial contrast-enhanced T1-weighted fat-saturated MR image shows peripheral nodular enhancement (arrow). Biopsy findings confirmed a low-grade chondrosarcoma.

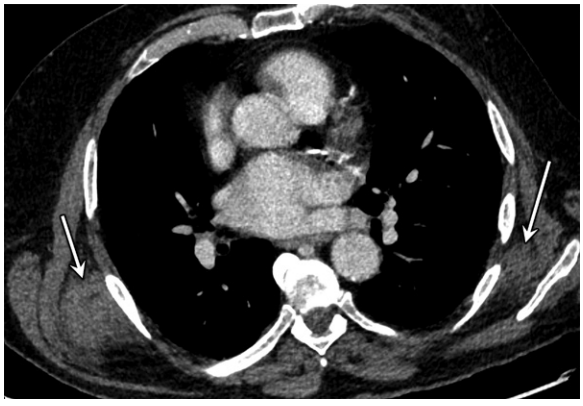

**Figure 12.** Elastofibroma dorsi in a 35-year-old man with right chest and back pain. Transaxial contrast-enhanced chest CT image shows bilateral well-circumscribed soft-tissue–attenuation masses with linear areas of interspersed fat (ie, lasagna sign) (arrows) in the posterior chest wall, deep to the latissimus dorsi and anterior to the scapular tip. The right mass was causing pain and discomfort and thus was removed. Histologic analysis confirmed elastofibroma dorsi.

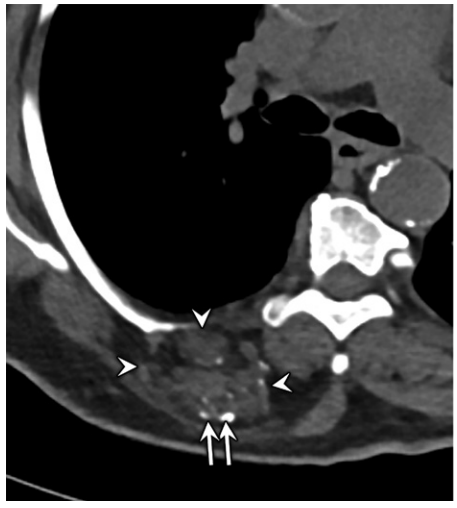

**Figure 13.** Hemangioma in a 73-year-old woman who underwent noncontrast CT before coronary artery bypass graft placement. Transaxial CT image shows a soft-tissue lesion (arrowheads) in the right posterior chest wall, with interspersed areas of internal fat and calcifications (arrows), representing phleboliths.

when the lesions are bilateral, with attenuation and texture similar to those of skeletal muscle. Elastofibroma dorsi lesions may be mildly T2 hyperintense, particularly on fat-suppressed MR images. Elastofibroma dorsi typically has linear areas of fat within the tumor, which are sometimes termed the *lasagna sign* because of the layering appearance (Fig 12) (41). It should be noted that while the area between the serratus anterior and the scapula is the most common location of elastofibroma dorsi lesions, they may occur less commonly at other sites in the thorax, with the second most common site being posterior to the first or second rib and deep to the superior scapula (42). The lesion may show very mild FDG uptake and mild enhancement (41). Elastofibroma dorsi is considered a "do not touch" lesion, for which the diagnosis can be confidently made with imaging alone, especially when the lesions are bilateral, with no need for biopsy or resection unless the patient is symptomatic. If the mass is large or shows intense contrast enhancement that renders making a diagnosis difficult, percutaneous biopsy could be performed for confirmation.

Vascular malformations can occasionally be seen in the chest wall and can be cutaneous, subcutaneous, intermuscular, or intramuscular (43). The most common type is the venous malformation, with the common misnomer of "cavernous hemangioma" (44). Venous malformations usually contain larger vessels that are

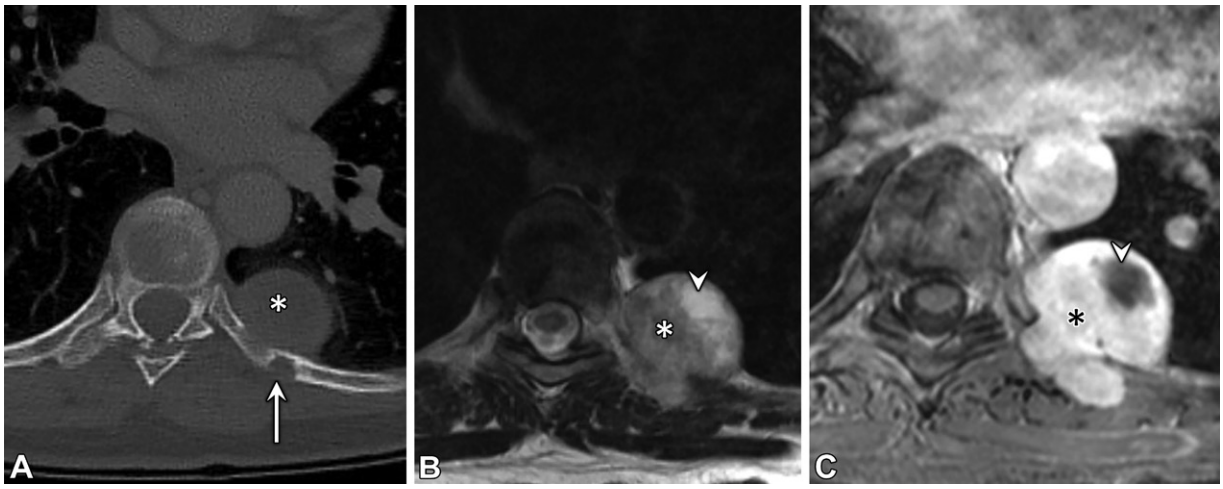


**Figure 14.** Schwannoma in a 59-year-old woman found to have a left posterior chest wall mass at CT performed for gallstone pancreatitis. **(A)** Transaxial contrast-enhanced CT image (bone window) shows the mass (*) adjacent to the left eighth rib, with a small area of bone remodeling (arrow). **(B)** Transaxial T2-weighted MR image shows a hyperintense bilobar mass (*) with a cystic area (arrowhead). **(C)** Transaxial contrast-enhanced T1-weighted fat-saturated MR image shows avid enhancement of the mass (*) , with no enhancement of the cystic area (arrowhead). Postresection histologic analysis confirmed a schwannoma.

seen as channels with flow voids on MR images. These malformations can also contain other tissue components, most notably phleboliths that result from dystrophic calcification of thrombi and macroscopic fat.

The presence of phleboliths on CT images is very suggestive of a hemangioma (Fig 13), as these calcific deposits occur in as many as 30% of venous malformations (45). Characteristic imaging findings of a hemangioma include areas of macroscopic fat, which appear hyperintense on T2- and T1-weighted MR images and are null on fat-suppressed MR images. Areas of low signal intensity can be seen and represent hemosiderin, septa, phleboliths, large vessels, or smooth muscle (46). After contrast material administration, hemangiomas demonstrate slow and gradual enhancement, with characteristic nodular enhancement of tortuous vessels and diffuse enhancement during the delayed phase (44).

## Nerve Sheath Tumors

The most common nerve sheath tumors are schwannomas and neurofibromas, with the former being far more common, representing 85% of chest nerve sheath tumors in one series (47). The main clue to the diagnosis of nerve sheath tumor is the location of the lesion. In the chest wall, these tumors usually arise from the intercostal nerves that course beneath the ribs (Fig 14) and can extend into and widen neural foramina (47,48). While most cases of neurofibromatosis type 1 involve neurofibromas, the majority of neurofibromas occur as isolated lesions.

It is important to note that neurofibromas are inseparable from the involved nerve; thus, resection of neurofibromas cannot be performed without resection of the nerve (49). This is not the case for schwannomas, which can be resected without sacrificing the nerve. At imaging, the nerve giving rise to the schwannoma can sometimes be seen coursing alongside the mass (49). Percutaneous biopsy of schwannomas can cause severe pain. It is important to note that schwannomas may show substantial uptake at FDG PET, with a maximal standardized uptake value as high as 8 (50). However, a benign neurofibroma should have, at most, mild uptake (51).

Neurofibroma and schwannoma occur in the same location and have overlapping findings. A few MRI findings can favor one diagnosis over the other. Approximately 50%–70% of neurofibromas may have a target sign, with a hypointense center surrounded by a hyperintense periphery, at T2-weighted MRI (Fig 15) (52). The central portion corresponds to fibrovascular tissue that also enhances after contrast medium administration, and the peripheral tissue corresponds to myxoid tissue (49,52). The fascicular sign on T2-weighted MR images, characterized by "rings" of hypointense areas, favors schwannoma (49,52). Larger schwannomas can develop areas of hemorrhage, necrosis, cyst formation, and/or calcification, which should not raise suspicion for malignant transformation (52).

Malignant peripheral nerve sheath tumors (MPNSTs) are important to identify in patients with neurofibromatosis type 1 because they are at increased risk for these tumors. The difficulty arises in patients who develop multiple plexiform neurofibromas. MPNST can also arise sporadically in patients who do not have neurofibromatosis type 1. Imaging findings that

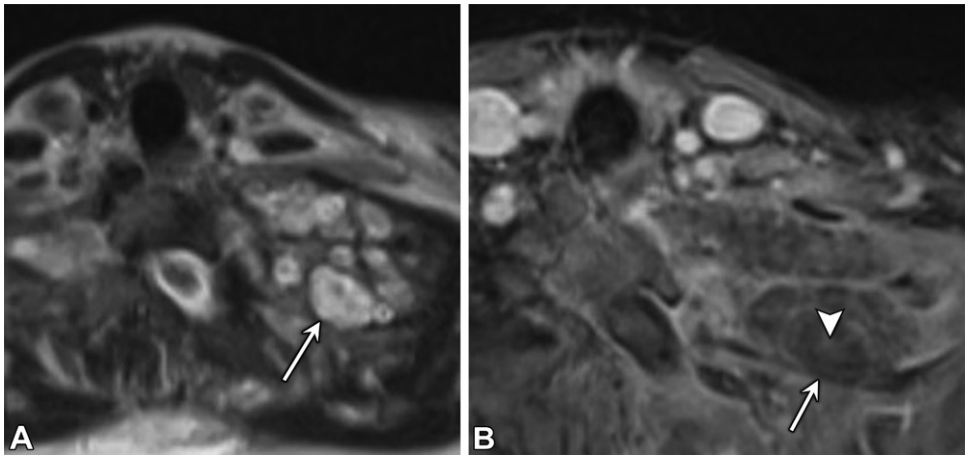


**Figure 15.** Known neurofibromatosis type 1 in a 19-year-old woman who underwent follow-up MRI for plexiform neurofibromas. **(A)** Transaxial T2-weighted MR image shows the target sign, with central low signal intensity and high peripheral signal intensity (arrow). **(B)** Transaxial contrast-enhanced T1-weighted fat-saturated MR image shows a plexiform neurofibroma (arrow), with enhancement of the central portion (arrowhead).

**Figure 16.** MPNST in an 11-year-old boy with a history of neurofibromatosis type 1, in whom radiography of the spine was performed for assessment of scoliosis. **(A)** Anteroposterior radiograph of the spine (right) shows a left chest wall mass (arrow) with increased size compared with its size on a chest radiograph obtained 1 year earlier (left). **(B)** Sagittal noncontrast CT image (bone window) shows the mass (arrow), with osseous destruction (arrowheads) of the adjacent ribs and transverse processes. **(C)** Coronal contrast-enhanced T1-weighted fat-saturated MR image shows a heterogeneously enhancing mass (arrow) with areas of necrosis. Biopsy findings confirmed MPNST.

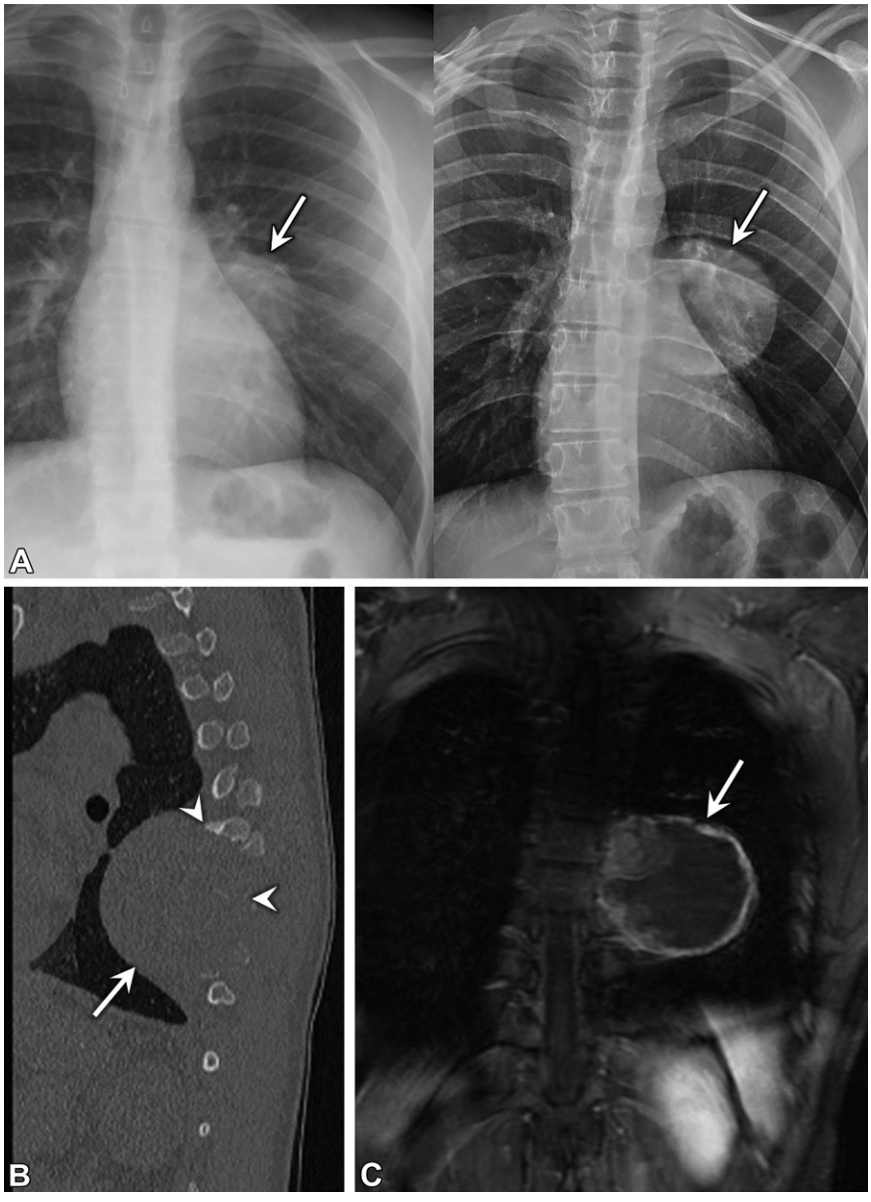

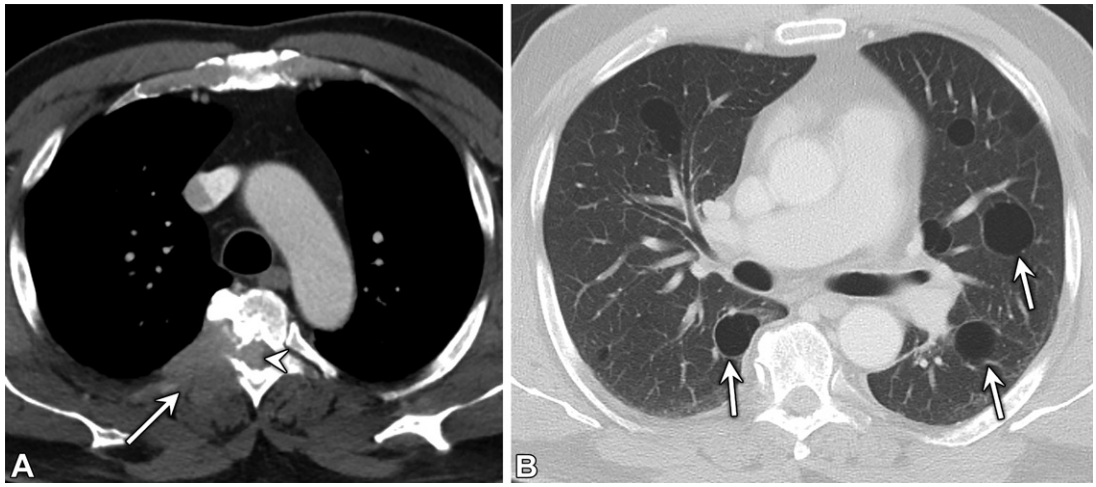


**Figure 17.** Myeloma in a 69-year-old man with lower extremity weakness. **(A)** Transaxial contrast-enhanced chest CT image (soft-tissue window) shows a right posterior chest wall mass (arrow) extending into the central canal (arrowhead). **(B)** Transaxial contrast-enhanced CT image (lung window) shows cysts (arrows) in both lungs secondary to amyloid involvement. Results of biopsy of the paraspinal mass confirmed multiple myeloma.

favor MPNST (Fig 16) include rapid growth, size larger than 5 cm, interval loss of the target or fascicular sign, infiltration into the surrounding soft tissues, adjacent osseous destruction, and evidence of distant metastasis (53,54). The appearances of MPNST can also overlap with those of other sarcomas.

## Malignant Lesions

Myeloma is an expansile bone lesion that can extend into the soft tissues. It is the most common primary bone marrow malignancy in adults (4). The most common locations of myeloma in the chest are the thoracic spine and the ribs (4). In addition to multiple myeloma, solitary myeloma, also known as a plasmacytoma, can arise in the bone or rarely, in soft tissues of the chest wall. In the majority of patients with solitary myeloma, progression to multiple myeloma occurs a few years after the diagnosis (4). CT shows the classic "punched-out" lytic lesions, which can expand the bone and erode the cortex. Rarely, light-chain deposition can result in cystic changes in the lungs (Fig 17), which when seen can help suggest the diagnosis of myeloma (55).

Lymphoma isolated to the chest wall is very rare. When present, chest wall lymphoma is often secondary to chest wall invasion by the mediastinal or axillary disease, or to extralymphatic spread in widely disseminated disease. Secondary chest wall involvement in lymphoma is typically due to Hodgkin disease or diffuse large B-cell lymphoma. On MR images, lymphoma demonstrates T1 hypointensity, T2 hyperintensity, and restricted diffusion (56).

Metastasis to the chest wall can occur by way of hematogenous dissemination or direct spread from adjacent thoracic tumors such as lung carcinoma, mesothelioma, breast cancer, and thymoma. In questionable cases, free-breathing cine MRI can be performed to confirm the presence of invasion, as sliding or independent movement of the parietal pleura against the mass excludes invasion (57). In women, breast cancer can recur in the chest wall within mastectomy or lumpectomy scars (58). If the primary tumor is not already known, a metastatic lesion in the chest wall can be targeted with US or CT guidance.

Aggressive fibromatosis, also known as desmoid tumor, consists of well-differentiated fibroblasts that develop from the connective tissues of the muscle, fascia, or scar from trauma or surgery. These tumors have a general predilection for the shoulder area. On images, they manifest as ill-defined and infiltrative masses. With aggressive fibromatosis, the mass is generally heterogeneous on CT images but can have the same attenuation as muscle; in these cases, the clue that a desmoid tumor is present is focal or asymmetric enlargement of a single muscle. While desmoid tumors usually are locally aggressive, they do not metastasize, and the presence of distant metastasis should suggest other neoplasms such as sarcoma.

At MRI, desmoid tumors are classically isointense to muscle on T1-weighted images and have intermediate or high signal intensity on T2-weighted images (Fig 18); however, their signal intensity characteristics are variable. T1- and T2-hypointense curvilinear and linear areas within the lesion also are characteristic (59). A chest wall mass with an appearance similar to that of muscle on CT and T1-weighted MR images should raise suspicion for desmoid tumor. Typically, these tumors require extensive chest wall resection, and

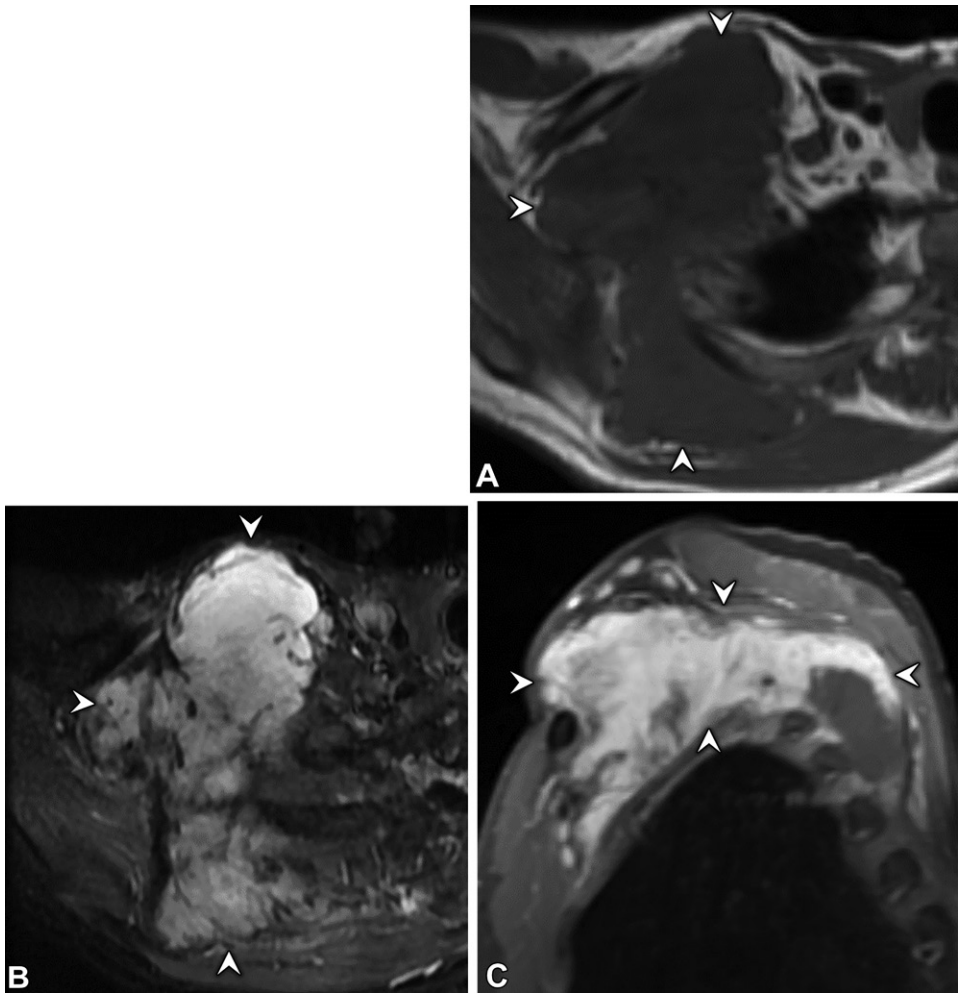


**Figure 18.** Aggressive fibromatosis (desmoid tumor) in a 55-year-old man with a history of Li-Fraumeni syndrome who presented with right shoulder pain. **(A, B)** Transaxial noncontrast T1-weighted **(A)** and short τ inversion-recovery **(B)** MR images show a T1-isointense (arrowheads in **A**) and T2-hyperintense (arrowheads in **B**) mass centered in the right shoulder, with invasion of the right scapula and right second and third ribs. **(C)** Coronal contrast-enhanced T1-weighted fat-saturated MR image shows avid enhancement (arrowheads). After multiple nondiagnostic biopsies, the mass was partially resected, and histopathologic analysis revealed a desmoid tumor.

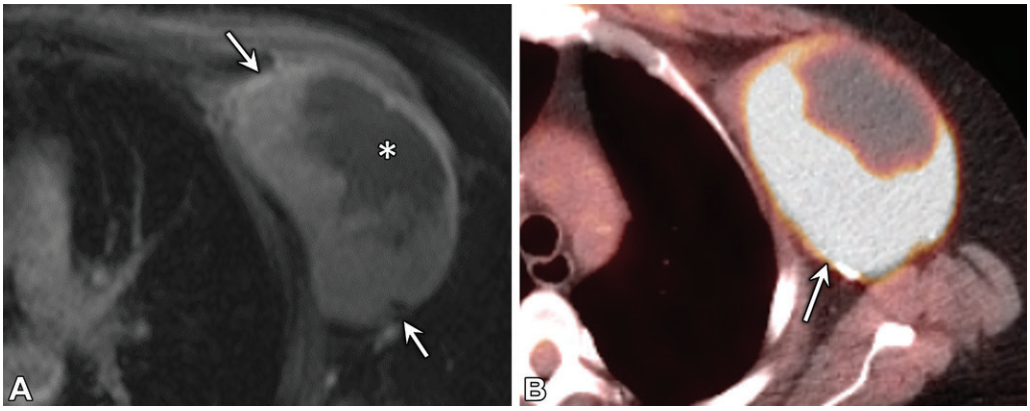


**Figure 19.** Undifferentiated pleomorphic sarcoma in a 59-year-old woman with a history of left breast cancer 22 years earlier and chemoradiation who presented with a palpable chest wall mass. **(A)** Transaxial contrast-enhanced T1-weighted fat-saturated MR image shows a mass (arrows) in the left subpectoral chest wall, with a cystic area (∗), likely representing necrosis. **(B)** Transaxial PET/CT image obtained later shows avid FDG uptake (arrow). Biopsy findings confirmed high-grade undifferentiated pleomorphic sarcoma.

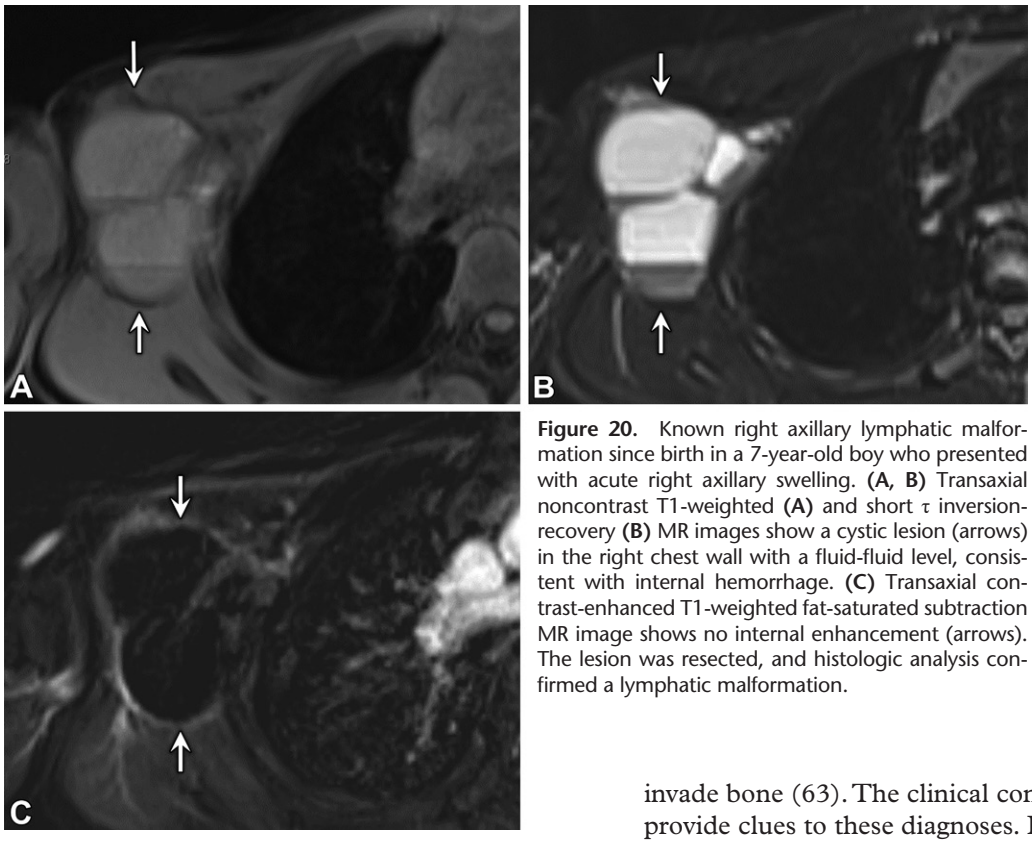


**Figure 20.** Known right axillary lymphatic malformation since birth in a 7-year-old boy who presented with acute right axillary swelling. **(A, B)** Transaxial noncontrast T1-weighted **(A)** and short τ inversion-recovery **(B)** MR images show a cystic lesion (arrows) in the right chest wall with a fluid-fluid level, consistent with internal hemorrhage. **(C)** Transaxial contrast-enhanced T1-weighted fat-saturated subtraction MR image shows no internal enhancement (arrows). The lesion was resected, and histologic analysis confirmed a lymphatic malformation.

they recur in up to 50% of cases (60). Tyrosine kinase inhibitors have shown promise in the treatment of this entity in recent years (61).

The most common primary malignant soft-tissue lesion of the chest wall in adults is undifferentiated pleomorphic sarcoma, formally known as malignant fibrous histiocytoma. These tumors usually occur in the deep fascia or skeletal muscle (Fig 19). Many of these soft-tissue sarcomas are difficult to differentiate with imaging and thus often require biopsy (17). However, the purpose of imaging is not to diagnose the tumor but rather to guide management and determine resectability. Also, certain clinical and imaging clues could favor certain diagnoses over others. For example, Ewing sarcoma of the chest wall should be the primary consideration in a pediatric patient who presents with a painful chest wall mass and fever. These tumors most commonly arise from the ribs, followed by the scapula, clavicle, and sternum. They can also arise in the soft tissues, especially in patients older than 20 years (62). At imaging, larger tumors are more prone to develop hemorrhage and necrosis (4).

Malignant vascular tumors include angiosarcoma and Kaposi sarcoma. These tumors tend to have a more superficial location in the subcutaneous tissues and at imaging manifest as skin thickening and subcutaneous fat stranding with an associated soft-tissue mass that occasionally may invade bone (63). The clinical context can also provide clues to these diagnoses. For example, patients with angiosarcoma may have a history of prior mastectomy, pulmonary parenchymal radiation change, and/or lymphedema. Patients with Kaposi sarcoma may have a history of organ transplantation or AIDS (63,64). On MR images, angiosarcoma appears as an intensely enhancing lesion with discrete vessels that cause flow voids along the periphery of the tumor (39).

## Fluid Lesions

### Cystic Neoplasms

Lymphatic malformations, formerly lymphangiomas, occur most commonly in the neck and axillary regions and consist of dilated lymphatic vessels. They usually have a cystic appearance and after contrast material administration may show thin peripheral and septal enhancement (Fig 20). On more delayed contrast-enhanced MR images, these lesions may show gradual increased enhancement owing to third spacing of contrast material within them (44). Lymphatic malformations are often quite infiltrative, extending through multiple thoracic compartments. There may be associated lymphatic edema in the lungs or chylous pleural effusions if the lesion is extensive. These lesions typically occur in children, although they can also be seen in young adults.

Aneurysmal bone cysts uncommonly occur in the chest wall. The most common location is the posterior elements of the spine and less commonly the posterior ribs. An aneurysmal bone cyst may

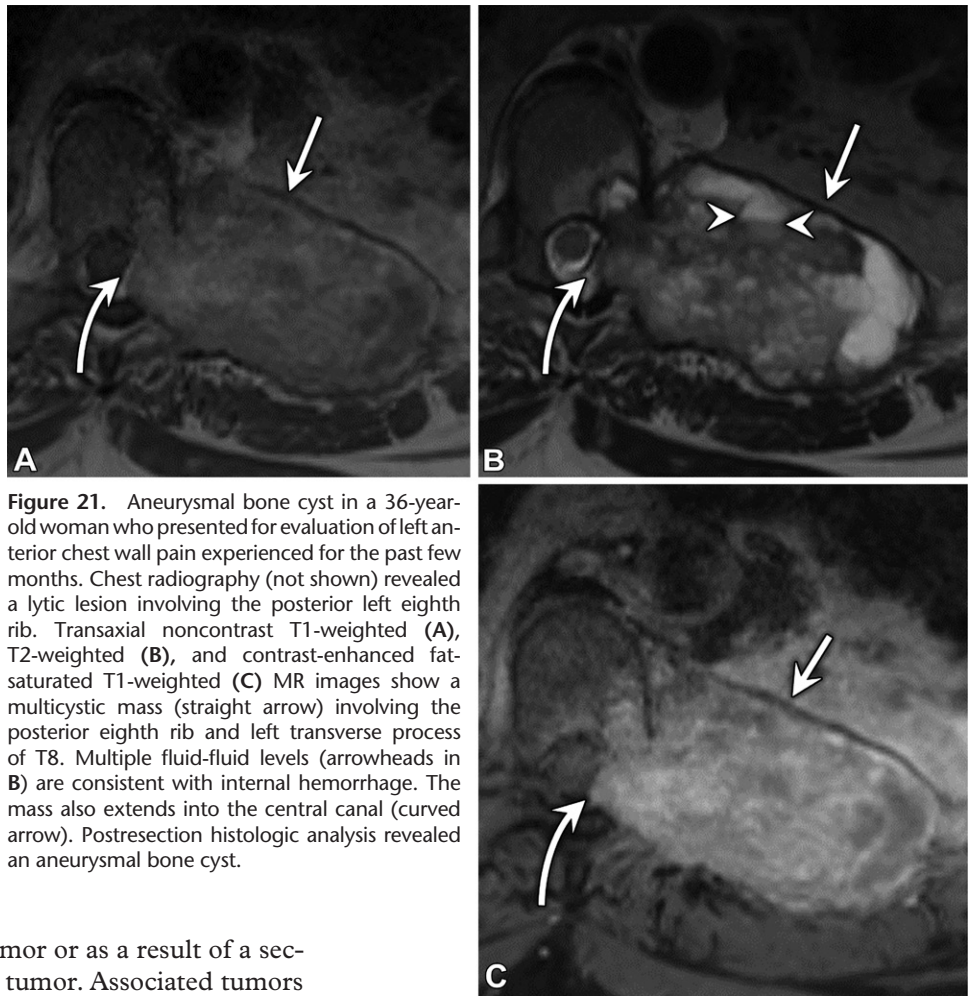


**Figure 21.** Aneurysmal bone cyst in a 36-year-old woman who presented for evaluation of left anterior chest wall pain experienced for the past few months. Chest radiography (not shown) revealed a lytic lesion involving the posterior left eighth rib. Transaxial noncontrast T1-weighted **(A)**, T2-weighted **(B)**, and contrast-enhanced fat-saturated T1-weighted **(C)** MR images show a multicystic mass (straight arrow) involving the posterior eighth rib and left transverse process of T8. Multiple fluid-fluid levels (arrowheads in **B**) are consistent with internal hemorrhage. The mass also extends into the central canal (curved arrow). Postresection histologic analysis revealed an aneurysmal bone cyst.

occur as a primary tumor or as a result of a secondary primary bone tumor. Associated tumors include chondromyxoid fibromas, chondrosarcomas, fibrous dysplasia, giant cell tumors, osteoblastomas, and osteosarcomas. Trauma is another possible cause of aneurysmal bone cysts (65). On MR images, these lesions are multiseptated and usually centered within the rib, with a well-defined hypointense rim (66). Fluid-fluid levels are highly suggestive of aneurysmal bone cysts and occur as a result of hemorrhage into the cystic spaces (Fig 21). Fluid-fluid levels are not pathognomonic and can also occur with other tumors, such as telangiectatic osteosarcoma and giant cell tumors with secondary aneurysmal bone cyst change (66).

It is important to note that many of the previously described neoplasms, such as schwannoma (67), necrotic metastases and sarcomas (4,68), and telangiectatic osteosarcoma (69), can develop cystic areas. The presence of nodular and enhancing soft tissue should raise suspicion for these entities.

## Nonneoplastic Lesions

Hematoma can occur with significant trauma, with minor trauma, or even spontaneously in patients who are on anticoagulation therapy or have coagulopathy. On CT images, hematomas appear as hyperattenuating collections, with the attenuation of acute blood measuring between 30 and 45 HU and the attenuation of clotted blood measuring 45–70 HU (70). In patients with anemia, clotted blood can have a lower attenuation (30 HU) (70).

While chest wall hematomas can be mistaken for a mass on CT and US images, MRI findings are often diagnostic of hematoma when a fluid-fluid level is seen within a fluid collection. The dependent layer, as compared with the nondependent layer, has higher T1 signal intensity and lower T2 signal intensity (Fig 22). In addition, hematomas may demonstrate a T1- and T2-hypointense rim owing to hemosiderin deposition. After contrast material administration, there is no enhancement of the collection itself, and this can easily be confirmed with subtraction images.

Enhancement of the wall is unusual for an acute hematoma and suggests a chronic or infected hematoma (38). Active bleeding into the hematoma is seen as a blush of contrast material extravasation within the hematoma that increases in size on more delayed images. Patients with active arterial hemorrhage may benefit from arterial

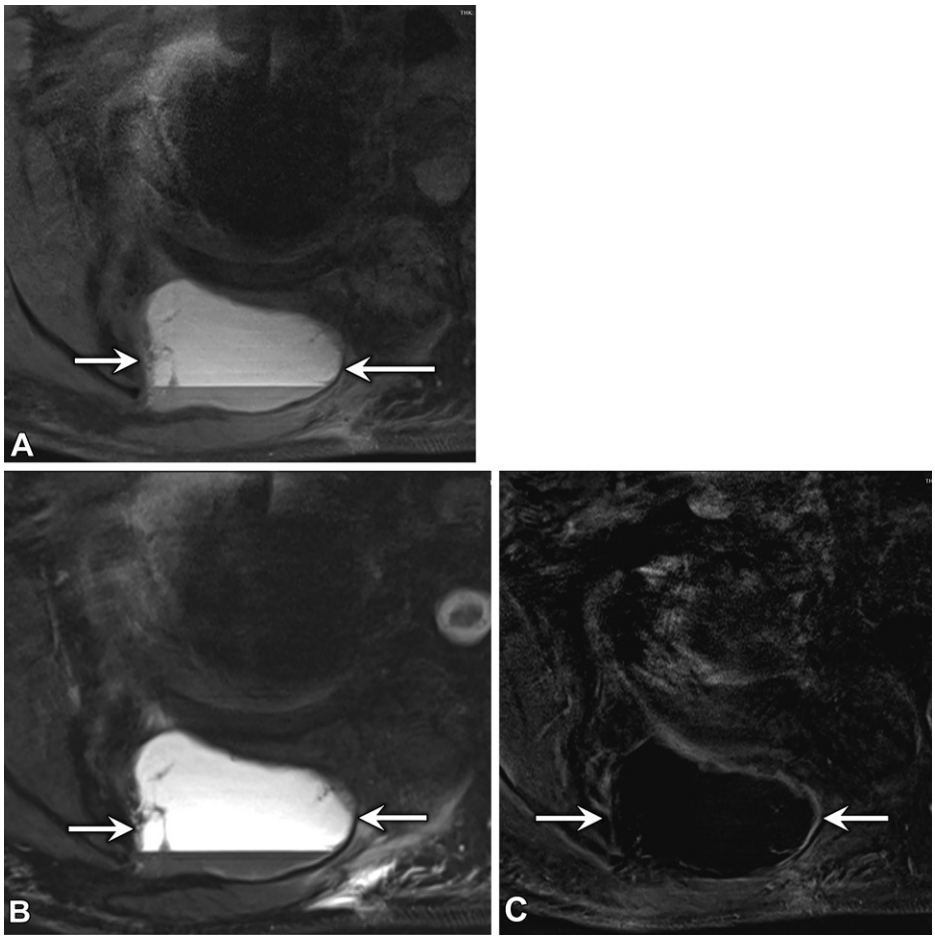


**Figure 22.** Hematoma in a 58-year-old man who underwent transaxial MRI after resection of a posterior chest wall desmoid tumor. **(A)** Noncontrast T1-weighted fat-saturated image shows a hyperintense fluid collection (arrows) with a fluid-fluid level at the resection site. **(B)** T2-weighted fat-saturated image shows the fluid collection (arrows), and similar to **A**, a relatively hypointense dependent layer. **(C)** Postcontrast fat-saturated T1-weighted subtraction image shows no enhancement (arrows), consistent with a hematoma. The collection was resolved at 6-month follow-up MRI.

embolization (71). It is important to note that chest wall tumors or metastases can lead to spontaneous hemorrhage. These lesions can be differentiated from benign hematoma by the presence of a solidly enhancing area within or adjacent to the hematoma on postcontrast subtraction MR images (38).

Infection of the chest wall is often misdiagnosed clinically. Patients at risk of developing chest wall infections include those who are immunocompromised, diabetic, posttraumatic, or intravenous drug users. The most commonly encountered organisms are *Staphylococcus aureus* and *Mycobacterium tuberculosis*. In patients who are immunocompromised or have diabetes, other less common pathogens, including fungal organisms, may be encountered, with *Aspergillus* species accounting for 80%–90% of fungal infections (72).

In intravenous drug users, abscesses commonly occur in the region of the sternoclavicular joint and sternochondral junction owing to attempts to inject a substance into the central veins of the neck. At CT, sternoclavicular septic arthritis manifests as an organized fluid collection that is centered in the joint space and may extend anteriorly into the soft tissue or posteriorly into the mediastinum (35). Fractured needle fragments in the soft tissues sometimes can be seen, and the surgeon or emergency physician should be notified of this in case an incision and drainage procedure is needed.

At imaging, abscesses appear as organized fluid collections with peripheral enhancement, often with surrounding fat stranding (Fig 23). Infection and a subsequent abscess develop by way of three mechanisms: direct inoculation into the skin after trauma or surgery, hematogenous spread, or direct extension from an intrathoracic infection (72). Chest wall extension from an intrathoracic infection is referred to as empyema necessitans and has been described in association

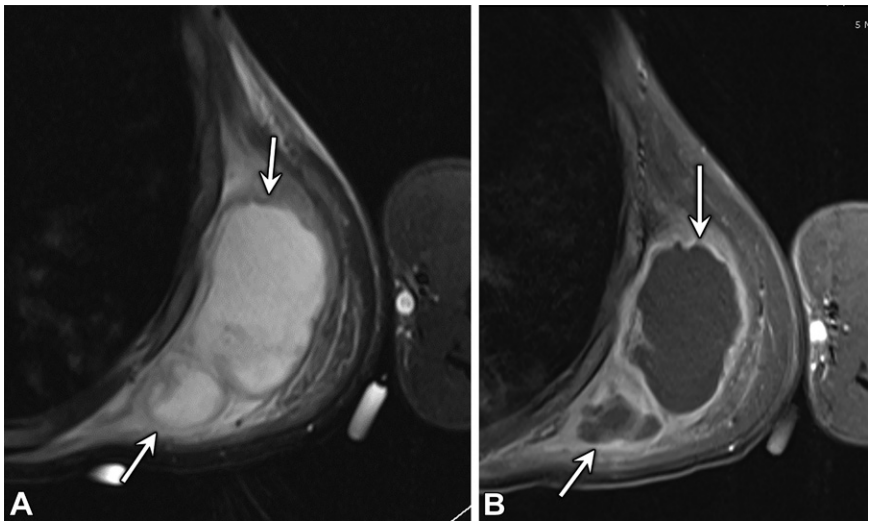


**Figure 23.** Abscess in a 33-year-old man with a history of common variable immunodeficiency who presented with fever and swelling. **(A)** Transaxial T2-weighted MR image reveals a loculated fluid collection (arrows) in the left chest wall. **(B)** Transaxial postcontrast T1-weighted fat-saturated MR image shows a thick rind of peripheral enhancement (arrows). Abscess was confirmed at surgical debridement.

with many pathogens, most notably *M tuberculosis*, *Actinomyces species*, *Nocardia species*, and *S aureus* (73,74).

The osseous thorax also can be involved, resulting in osteomyelitis, which manifests as osseous destruction on CT images and as marrow edema and enhancement on MR images. Imaging findings of osteomyelitis include osseous destruction without new bone formation, calcification in the wall of the abscess, and bone sequestrum in destroyed bone (75). Owing to its indolent clinical features and chronicity of infection, chest wall tuberculosis can be mistaken for a soft-tissue neoplasm. Biopsy may be needed to guide therapy or differentiate chest wall tuberculosis from a plasmacytoma or osseous metastasis.

## Conclusion

Chest wall lesions can be challenging for the cardiothoracic radiologist, as many of these lesions are not common and are musculoskeletal or neurogenic in origin. Still, the radiologist plays an important role in diagnosing and directing further workup and management of these lesions. An approach based on the location and predominant composition of the lesion on MR and CT images is of benefit in this regard. It is important to recognize and diagnose entities that are definitely benign and thus require no further workup and to distinguish them from lesions that are indeterminate or malignant and may require biopsy, resection, and/or medication treatment.

***Disclosures of conflicts of interest.*—S.B.** Member of RSNA Board of Directors. **M.H.** Editorial board member of *RadioGraphics*.

## References

1. Incarbone M, Pastorino U. Surgical treatment of chest wall tumors. World J Surg 2001;25(2):218–230.
2. Tateishi U, Gladish GW, Kusumoto M, et al. Chest wall tumors: radiologic findings and pathologic correlation. I. Benign tumors. RadioGraphics 2003;23(6):1477–1490.
3. Carter BW, Gladish GW. MR imaging of chest wall tumors. Magn Reson Imaging Clin N Am 2015;23(2):197–215.
4. Tateishi U, Gladish GW, Kusumoto M, et al. Chest wall tumors: radiologic findings and pathologic correlation. II. Malignant tumors. RadioGraphics 2003;23(6):1491–1508.
5. Bancroft LW, Kransdorf MJ, Peterson JJ, O'Connor MI. Benign fatty tumors: classification, clinical course, imaging appearance, and treatment. Skeletal Radiol 2006;35(10):719–733.
6. Matsumoto K, Hukuda S, Ishizawa M, Chano T, Okabe H. MRI findings in intramuscular lipomas. Skeletal Radiol 1999;28(3):145–152.
7. Mehregan DR, Mehregan DA, Mehregan AH, Dorman MA, Cohen E. Spindle cell lipomas: a report of two cases—one with multiple lesions. Dermatol Surg 1995;21(9):796–798.
8. Lee JC, Gupta A, Saifuddin A, et al. Hibernoma: MRI features in eight consecutive cases. Clin Radiol 2006;61(12):1029–1034.
9. Kok KY, Telisinghe PU. Lipoblastoma: clinical features, treatment, and outcome. World J Surg 2010;34(7):1517–1522.
10. Alaggio R, Coffin CM, Weiss SW, et al. Liposarcomas in young patients: a study of 82 cases occurring in patients younger than 22 years of age. Am J Surg Pathol 2009;33(5):645–658.
11. Chan LP, Gee R, Keogh C, Munk PL. Imaging features of fat necrosis. AJR Am J Roentgenol 2003;181(4):955–959.
12. Lee SA, Chung HW, Cho KJ, et al. Encapsulated fat necrosis mimicking subcutaneous liposarcoma: radiologic findings on MR, PET-CT, and US imaging. Skeletal Radiol 2013;42(10):1465–1470.
13. Murphey MD, Arcara LK, Fanburg-Smith J. From the archives of the AFIP: imaging of musculoskeletal liposarcoma with radiologic-pathologic correlation. RadioGraphics 2005;25(5):1371–1395.
14. Moch H. Soft tissue and bone tumours. In: WHO classification of tumours, Vol 3. Geneva, Switzerland: World Health Organization, 2020; 3.
15. Kransdorf MJ, Bancroft LW, Peterson JJ, Murphey MD, Foster WC, Temple HT. Imaging of fatty tumors: distinction

of lipoma and well-differentiated liposarcoma. Radiology 2002;224(1):99–104.
16. Murphey MD. World Health Organization classification of bone and soft tissue tumors: modifications and implications for radiologists. Semin Musculoskelet Radiol 2007;11(3):201–214.
17. Lee TJ, Collins J. MR imaging evaluation of disorders of the chest wall. Magn Reson Imaging Clin N Am 2008;16(2):355–379, x.
18. Waller DA, Newman RJ. Primary bone tumours of the thoracic skeleton: an audit of the Leeds regional bone tumour registry. Thorax 1990;45(11):850–855.
19. Anderson BO, Burt ME. Chest wall neoplasms and their management. Ann Thorac Surg 1994;58(6):1774–1781.
20. Jee WH, Choi KH, Choe BY, Park JM, Shinn KS. Fibrous dysplasia: MR imaging characteristics with radiopathologic correlation. AJR Am J Roentgenol 1996;167(6):1523–1527.
21. Czajka CM, DiCaprio MR. What is the proportion of patients with multiple hereditary exostoses who undergo malignant degeneration? Clin Orthop Relat Res 2015;473(7):2355–2361.
22. Pedrini E, Jennes I, Tremosini M, et al. Genotype-phenotype correlation study in 529 patients with multiple hereditary exostoses: identification of "protective" and "risk" factors. J Bone Joint Surg Am 2011;93(24):2294–2302.
23. Murphey MD, Choi JJ, Kransdorf MJ, Flemming DJ, Gannon FH. Imaging of osteochondroma: variants and complications with radiologic-pathologic correlation. RadioGraphics 2000;20(5):1407–1434.
24. Bernard SA, Murphey MD, Flemming DJ, Kransdorf MJ. Improved differentiation of benign osteochondromas from secondary chondrosarcomas with standardized measurement of cartilage cap at CT and MR imaging. Radiology 2010;255(3):857–865.
25. Murphey MD, Sartoris DJ, Quale JL, Pathria MN, Martin NL. Musculoskeletal manifestations of chronic renal insufficiency. RadioGraphics 1993;13(2):357–379.
26. Banks KP, Bui-Mansfield LT, Chew FS, Collinson F. A compartmental approach to the radiographic evaluation of soft-tissue calcifications. Semin Roentgenol 2005;40(4):391–407.
27. Kransdorf MJ, Meis JM. From the archives of the AFIP. Extraskeletal osseous and cartilaginous tumors of the extremities. RadioGraphics 1993;13(4):853–884.
28. Cortellazzo Wiel L, Trevisan M, Murru FM, Rabusin M, Barbi E. Myositis ossificans mimicking sarcoma: a not so rare bioptic diagnostic pitfall. Ital J Pediatr 2020;46(1):110.
29. Łuczyńska E, Kasperkiewicz, Domalik A, Cwierz A, Bobek-Billewicz B. Myositis ossificans mimicking sarcoma, the importance of diagnostic imaging: case report. Pol J Radiol 2014;79:228–232.
30. Valenzuela A, Song P, Chung L. Calcinosis in scleroderma. Curr Opin Rheumatol 2018;30(6):554–561.
31. Bouros D, Wells AU, Nicholson AG, et al. Histopathologic subsets of fibrosing alveolitis in patients with systemic sclerosis and their relationship to outcome. Am J Respir Crit Care Med 2002;165(12):1581–1586.
32. Dalakas MC, Hohlfeld R. Polymyositis and dermatomyositis. Lancet 2003;362(9388):971–982.
33. Chen IJ, Jan Wu YJ, Lin CW, et al. Interstitial lung disease in polymyositis and dermatomyositis. Clin Rheumatol 2009;28(6):639–646.
34. Tornling G, Lundberg IE. Pulmonary involvement in polymyositis and dermatomyositis. Int J Clin Rheumatol 2009;4(1):45–56.
35. Restrepo CS, Martinez S, Lemos DF, et al. Imaging appearances of the sternum and sternoclavicular joints. RadioGraphics 2009;29(3):839–859.
36. Earwaker JW, Cotten A. SAPHO: syndrome or concept? Imaging findings. Skeletal Radiol 2003;32(6):311–327.
37. Firinu D, Garcia-Larsen V, Manconi PE, Del Giacco SR. SAPHO syndrome: current developments and approaches to clinical treatment. Curr Rheumatol Rep 2016;18(6):35.
38. Mullan CP, Madan R, Trotman-Dickenson B, Qian X, Jacobson FL, Hunsaker A. Radiology of chest wall masses. AJR Am J Roentgenol 2011;197(3):W460–W470.
39. Nam SJ, Kim S, Lim BJ, et al. Imaging of primary chest wall tumors with radiologic-pathologic correlation. RadioGraphics 2011;31(3):749–770.
40. Berquist TH. Magnetic resonance imaging of primary skeletal neoplasms. Radiol Clin North Am 1993;31(2):411–424.
41. Battaglia M, Vanel D, Pollastri P, et al. Imaging patterns in elastofibroma dorsi. Eur J Radiol 2009;72(1):16–21.
42. Ochsner JE, Sewall SA, Brooks GN, Agni R. Best cases from the AFIP: elastofibroma dorsi. RadioGraphics 2006;26(6):1873–1876.
43. Murphey MD, Fairbairn KJ, Parman LM, Baxter KG, Parsa MB, Smith WS. From the archives of the AFIP: musculoskeletal angiomatous lesions—radiologic-pathologic correlation. RadioGraphics 1995;15(4):893–917.
44. Flors L, Leiva-Salinas C, Maged IM, et al. MR imaging of soft-tissue vascular malformations: diagnosis, classification, and therapy follow-up. RadioGraphics 2011;31(5):1321–1340; discussion 1340–1341.
45. Levine E, Wetzel LH, Neff JR. MR imaging and CT of extrahepatic cavernous hemangiomas. AJR Am J Roentgenol 1986;147(6):1299–1304.
46. Jeung MY, Gangi A, Gasser B, et al. Imaging of chest wall disorders. RadioGraphics 1999;19(3):617–637.
47. Yamaguchi M, Yoshino I, Fukuyama S, et al. Surgical treatment of neurogenic tumors of the chest. Ann Thorac Cardiovasc Surg 2004;10(3):148–151.
48. Ribet ME, Cardot GR. Neurogenic tumors of the thorax. Ann Thorac Surg 1994;58(4):1091–1095.
49. Kehoe NJ, Reid RP, Semple JC. Solitary benign peripheral-nerve tumours: review of 32 years' experience. J Bone Joint Surg Br 1995;77(3):497–500.
50. Dewey BJ, Howe BM, Spinner RJ, et al. FDG PET/CT and MRI features of pathologically proven schwannomas. Clin Nucl Med 2021;46(4):289–296.
51. Bredella MA, Torriani M, Hornicek F, et al. Value of PET in the assessment of patients with neurofibromatosis type 1. AJR Am J Roentgenol 2007;189(4):928–935.
52. Jee WH, Oh SN, McCauley T, et al. Extraaxial neurofibromas versus neurilemmomas: discrimination with MRI. AJR Am J Roentgenol 2004;183(3):629–633.
53. Wasa J, Nishida Y, Tsukushi S, et al. MRI features in the differentiation of malignant peripheral nerve sheath tumors and neurofibromas. AJR Am J Roentgenol 2010;194(6):1568–1574.
54. Yun JS, Lee MH, Lee SM, et al. Peripheral nerve sheath tumor: differentiation of malignant from benign tumors with conventional and diffusion-weighted MRI. Eur Radiol 2021;31(3):1548–1557.
55. Clayden RC, Macdonald D, Oikonomou A, Cheung MC. Cystic lung disease with kappa light chain deposition in newly diagnosed multiple myeloma. Br J Haematol 2020;188(2):201.
56. Knisely BL, Broderick LS, Kuhlman JE. MR imaging of the pleura and chest wall. Magn Reson Imaging Clin N Am 2000;8(1):125–141.
57. Sakai S, Murayama S, Murakami J, Hashiguchi N, Masuda K. Bronchogenic carcinoma invasion of the chest wall: evaluation with dynamic cine MRI during breathing. J Comput Assist Tomogr 1997;21(4):595–600.
58. O'Sullivan P, O'Dwyer H, Flint J, Munk PL, Muller N. Soft tissue tumours and mass-like lesions of the chest wall: a pictorial review of CT and MR findings. Br J Radiol 2007;80(955):574–580.
59. Kransdorf MJ, Jelinek JS, Moser RP Jr, et al. Magnetic resonance appearance of fibromatosis: a report of 14 cases and review of the literature. Skeletal Radiol 1990;19(7):495–499.
60. Allen PJ, Shriver CD. Desmoid tumors of the chest wall. Semin Thorac Cardiovasc Surg 1999;11(3):264–269.
61. Szucs Z, Messiou C, Wong HH, et al. Pazopanib, a promising option for the treatment of aggressive fibromatosis. Anticancer Drugs 2017;28(4):421–426.
62. Gladish GW, Sabloff BM, Munden RF, Truong MT, Erasmus JJ, Chasen MH. Primary thoracic sarcomas. RadioGraphics 2002;22(3):621–637.
63. Restrepo CS, Martínez S, Lemos JA, et al. Imaging manifestations of Kaposi sarcoma. RadioGraphics 2006;26(4):1169–1185.

64. Coldwell DM, Baron RL, Charnsangavej C. Angiosarcoma. Diagnosis and clinical course. Acta Radiol 1989;30(6):627–631.
65. Stevens KJ, Stevens JA. Aneurysmal bone cysts. Treasure Island, Fla: StatPearls Publishing; 2020.
66. Beltran J, Simon DC, Levy M, Herman L, Weis L, Mueller CF. Aneurysmal bone cysts: MR imaging at 1.5 T. Radiology 1986;158(3):689–690.
67. Kumar S, Gupta R, Handa A, Sinha R. Totally cystic intradural schwannoma in thoracic region. Asian J Neurosurg 2017;12(1):131–133.
68. Braham E, Aloui S, Aouadi S, Drira I, Kilani T, El Mezni F. Synovial sarcoma of the chest wall: a case report and literature review. Ann Transl Med 2013;1(1):9.
69. Liu JJ, Liu S, Wang JG, et al. Telangiectatic osteosarcoma: a review of literature. OncoTargets Ther 2013;6:593–602.
70. Lee JK. Computed body tomography with MRI correlation. Philadelphia, Pa: Lippincott Williams & Wilkins, 2006.
71. Dohan A, Darnige L, Sapoval M, Pellerin O. Spontaneous soft tissue hematomas. Diagn Interv Imaging 2015;96(7-8):789–796.
72. Chelli Bouaziz M, Jelassi H, Chaabane S, Ladeb MF, Ben Miled-Mrad K. Imaging of chest wall infections. Skeletal Radiol 2009;38(12):1127–1135.
73. Kono SA, Nauser TD. Contemporary empyema necessitatis. Am J Med 2007;120(4):303–305.
74. Kanne JP, Yandow DR, Mohammed TLH, Meyer CA. CT findings of pulmonary nocardiosis. AJR Am J Roentgenol 2011;197(2):W266–W272.
75. Shah J, Patkar D, Parikh B, et al. Tuberculosis of the sternum and clavicle: imaging findings in 15 patients. Skeletal Radiol 2000;29(8):447–453.